What's Wrong with Collision Detection in Multibody Dynamics Simulation?*

Daniel Montrallo Flickinger[1] and Jedediyah Williams[1] and Jeffrey C. Trinkle[1]

Abstract— **Contemporary time-stepping methods used in the dynamic simulation of rigid bodies suffer from problems in accuracy, performance, and robustness. Significant allowances for tuning, coupled with careful implementation of a broad phase collision detection scheme is required to make dynamic simulation useful for practical applications. A recently developed formulation method is presented herein that is more robust, and not dependent on broad-phase collision detection or system tuning for its behavior.**

Several uncomplicated benchmark examples are presented to give an analysis and make a comparison of the new Polyhedral Exact Geometry time-stepping method with the well-known Stewart-Trinkle time-stepping method. The behavior and performance for the two methods are discussed. This includes specific cases where contemporary time-steppers fail, and how they are ameliorated by the new method presented here. The goal of this work is to complete the groundwork for further research into high performance simulation.

I. Introduction

Multibody dynamic simulation is used in a broad range of engineering, research, and entertainment fields. The demand for fast and accurate simulation is high, as dynamic problems grow larger and larger under limited computation power. The work presented herein is the development of a time-stepping method for dynamic simulation intended to push the boundaries of robustness, performance, and accuracy. Accurate simulation of the motion of machinery is crucial in mechanical design [1], [2], [3]. It is particularly useful in designing complex machinery that is expensive to prototype, such as internal combustion engines [4]. Accurate simulation is required for robotics applications, particularly where contact is expected, such as in grasp planning [5]. And virtual reality is more useful and convincing when objects undergo more realistic motion in simulation [6]. Entertainment products such as motion pictures and video games benefit from accurate simulation [7], where realism is enhanced.

Simulation of the dynamics of multibody systems has traditionally involved a rigid body model with Coulomb friction; with unilateral constraints described by complementarity conditions [8], [9], [10]. The field is rooted further on the study of classical mechanics [11]. Computer simulation of multibody systems is related to work in the computer graphics field, with polyhedral models of objects common [12], [13], [14], and contact generally modeled as occurring between topologically connected features such as vertices, edges, and faces. In common practice, the contact model between vertex and face is used to prevent penetration.

Commonly used time-stepping methods are classified as either prevention, or correction methods. Correction methods consider only pairs of objects that are touching or in penetration during each timestep [15], [16], [17]. Current constraint violations are kept from becoming worse, but can take multiple timesteps to correct. This affects the overall accuracy of the simulation, as error from penetration is unavoidable without adjusting timestep length and affecting simulation performance. All popular physics engines employ correction type methods because common collision detection methods are designed only to consider current penetration.

Prevention methods form constraints for pairs of objects which could collide in the following timestep [18], [19], [20]. These methods have fewer penetrations, and can avoid undesirable effects such as tunneling without having to adjust the length of timesteps for specific system states. The Polyhedral Exact Geometry method is of the prevention method class.

Popular physics engines such as PhysX [21], and Bullet [7] use variations of the Stewart-Trinkle [18], [22] and Anitescu-Potra [17], [23] methods. The errors of the constraints in non-convex freespaces is mitigated in these programs by using a broad-phase collision detection algorithm considering only features within a small distance, ϵ of each other. This method bounds the error, but does not eliminate it completely. Further, it requires shorter timesteps as ϵ decreases, which requires more steps and increases total simulation time. The common methods discussed in this work assume that all bodies are convex. In cases where non-convex bodies exist, they are decomposed into adjoining convex bodies [24], [25]. The bodies can be decomposed, but the freespace cannot. The research presented herein continues the work in [26].

II. Methods

A. Equations of Motion

Rigid bodies in simulation move in accordance with the equations of motion. In the systems considered in this paper, the Newton-Euler equations are used in the dynamics formulation,

$$\mathbf{M}(\mathbf{q},\mathrm{t})\dot{\mathbf{v}} = \lambda_{\mathrm{vp}}(\mathbf{q},\dot{\mathbf{q}},\mathrm{t}) + \lambda_{\mathrm{app}}, \tag{1}$$

where λ_{vp} is the sum of velocity dependent forces, and λ_{app} are the applied forces. The system is subject to the

*This work was supported by NSF CCF-1208468 and DARPA W15P7T-12-1-0002. Any opinions, findings, and conclusions or recommendations expressed in this material are those of the authors and do not necessarily reflect the views of the funding agencies.

[1]Department of Computer Science, Rensselaer Polytechnic Institute { dmflickinger, jedediyah, trinkle } at gmail.com

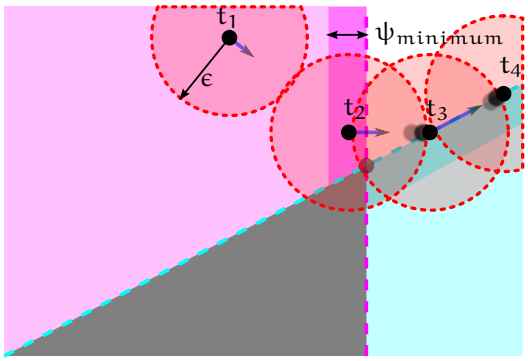

Fig. 1: *Vertex at times $t_1 \ldots t_4$ moving within the constraint half-spaces near an object, Stewart-Trinkle method*

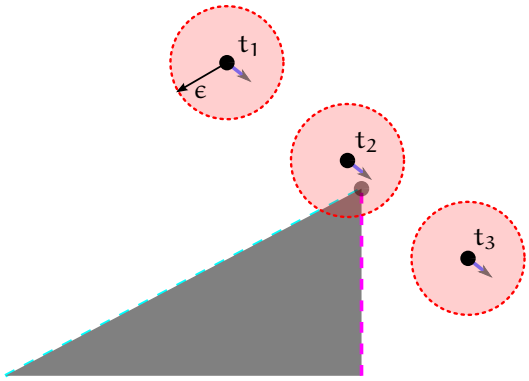

Fig. 2: *Vertex at times $t_1 \ldots t_3$ moving in proximity to an object, Polyhedral Exact Geometry method*

complementarity constraint,

$$0 \leq \lambda_n^{l+1} \perp \mathbf{G}_n^T v^{l+1} + \frac{\psi_n^l}{h} + \frac{\partial \psi_n^l}{\partial t} \geq 0, \tag{2}$$

where λ_n are forces normal to contact surfaces, Ψ_n are gap functions, or distances between active bodies and contact surfaces, h is the step size, v are the velocities of the active bodies, and $\mathbf{G}_n$ is a normal contact wrench.

B. Broad phase collision detection

A broad phase collision detection scheme is utilized to avoid the need to include all possible contact constraints at every time step. In the specific implementation discussed herein, if any edge in a body is closer than a predetermined value ϵ to the particle, then all edge constraints in that body are added to the formulation for the current time step. ϵ can be calculated as a function of particle velocity, or tuned for specific systems. In the examples presented Section III, ϵ is set to a large value in order to illustrate the differences between solution methods.

The inclusion of the tunable parameter ϵ can cause undesirable behavior when used in conjunction with the Stewart-Trinkle method. Figure 1 illustrates a case where an object picks up additional kinetic energy from interacting with constraints extended beyond the actual boundary of the object.

A particle moving in two dimensional space is represented as a black dot. The gray area represents an adjoining object; and the particle should be prevented from penetrating it. The two edges, represented by cyan and magenta dashed lines create the shaded half-spaces in their corresponding colors. These depict the region of the unilateral constraints. A red sphere, with a dashed line represents the bubble around the object within range of ϵ.

The active object is shown at several time-steps. Starting at t_1, the object has a velocity down and to the right, as indicated by the arrow. At this time, the adjoining object is outside the sphere of radius ϵ, and therefore no constraints are active. At t_2, the adjoining object is within the ϵ bubble, and now both constraints are active. Because this event occurred within a single time-step, the magenta constraint is now violated. This penetration causes a large spike in velocity. The object hits the cyan constraint at the next time-step t_3, and proceeds to follow the boundary even though the true edge of the non-active object is not in this region. At t_4, the active object has traveled at high velocity, and the other object has crossed outside the ϵ bubble. Now unconstrained, it proceeds at high velocity up and to the right of the figure. This behavior is seen later in Figure 5.

The energy gain can be partially mitigated by defining the parameter $\psi_{minimum}$. This parameter is represented by darker regions on the half-spaces. This allows the simulation to ignore constraints in deep penetration, which cause large energy gains.

Figure 2 demonstrates the behavior of the system under the Polyhedral Exact Geometry method. The two constraints become active at t_2 as the active object comes with distance ϵ of the non-active object. But the constraints do not alter the behavior of the active object, as they conform to the actual geometry of the non-active object.

C. Formulation of the Mixed Linear Complementarity Problem

Equations (1) and (2) are formulated as a mixed linear complementarity problem [27], [28], using the Stewart-Trinkle formulation,

$$\begin{vmatrix} 0 \\ \rho_n^{l+1} \end{vmatrix} = \begin{vmatrix} M & -G_n \\ G_n^T & 0 \end{vmatrix} \begin{vmatrix} v^{l+1} \\ p_n^{l+1} \end{vmatrix} + \begin{vmatrix} -Mv^l - p_{ext}^l \\ \psi_n^l/h \end{vmatrix}, \tag{3}$$

where M is the block diagonal mass matrix of all active bodies in the system, v is the generalized velocities, p_n and p_{ext} are normal and external impulsive forces, and h is the time step. The normal contact wrench is defined as

$$G_{n_{ij}} = \begin{bmatrix} \hat{n}_{ij} \\ r_{ij} \times \hat{n}_{ij} \end{bmatrix}, \tag{4}$$

which is indexed over k collisions by the i^{th} body and j^{th} collision. Friction is omitted from the formulation for clarity. The term r is the position vector from the center of mass of the body to the point on the body in collision with another object. $\hat{n}$ is a unit vector in the direction normal from the surface in collision.

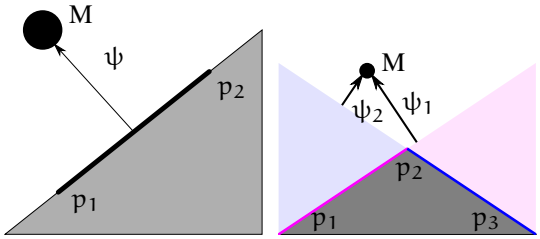

Fig. 3: *Particle M interacting with a single and double edge*

The problem size for the Stewart-Trinkle method is $2 \cdot n_b + n_c$, where n_b is the number of active bodies, and n_c is the number of contacts [18].

D. A particle with a single contact constraint

Consider a particle, M, moving in $\Re^2$ space with a single edge, with configuration $\mathbf{q}$ at time t, as depicted in Figure 3. A single edge is present in the space, bounded by vertices p_1 and p_2. This edge presents a unilateral constraint to the particle. That is, the particle is free to move on one side of the edge, but not on the other. The gap distance of the particle is represented as ψ_n, and is a function of the configuration at the current time. It is positive in the direction normal to the edge into the free space.

This unilateral constraint from (2) is represented as the complementarity condition,

$$0 \leq \lambda_n \perp \psi_n(\mathbf{q}, t) \geq 0, \tag{5}$$

where λ_n is the force on the particle, normal to the edge, to keep the particle from crossing the boundary.

The constraint in (5) is valid if the edge is of infinite length. But in this example, the edge is a line segment between two vertices in $\Re^2$ space.

E. A particle with two contact constraints

An additional vertex is added to the system in Figure 3. The area above the two edges is the free space of the particle. The area in gray is a solid body that the particle is constrained from penetrating.

The constraints produced by the edges comprise two half-spaces, of which are depicted with corresponding colors. If two constraints in the form in (5) are included in the formulation, the free-space for the particle in simulation will be restricted to the white region only.

To prevent penetration of the body while allowing penetration into the half-spaces outside the body, the constraint

$$\max(\psi_1, \psi_2) \geq 0 \tag{6}$$

is proposed [26]. That is, only the constraint with the maximum gap distance should be active at any given time. Consider the relation

$$\max(\psi_1, \psi_2) = \psi_2 + \max(0, \psi_1 - \psi_2). \tag{7}$$

Defining

$$c = \max(0, \psi_1 - \psi_2) \tag{8}$$

results in the complementarity constraint

$$0 \leq c - (\psi_1 - \psi_2) \perp c \geq 0. \tag{9}$$

The remaining constraints are defined by

$$0 \leq \max(\psi_1, \psi_2) \perp \lambda_1 \geq 0 \tag{10}$$
$$0 \leq \max(\psi_1, \psi_2) \perp \lambda_2 \geq 0, \tag{11}$$

which for this example give

$$0 \leq c + \psi_2 \perp \lambda_1 \geq 0 \tag{12}$$
$$0 \leq c + \psi_2 \perp \lambda_2 \geq 0. \tag{13}$$

F. General Polyhedral Exact Geometry Formulation

Expanding the constraint in (9), a general system with m facets in contact is realized,

$$\begin{aligned}
0 \leq c_2 - \psi_2 + \psi_1 \perp c_2 \geq 0 \\
0 \leq c_3 - \psi_3 + c_2 + \psi_1 \perp c_3 \geq 0 \\
\vdots \\
0 \leq c_m - \psi_m + c_m + c_{m-1} + \ldots + c_2 + \psi_1 \perp c_m \geq 0
\end{aligned} \tag{14}$$

$$\begin{aligned}
0 \leq d_1 + \psi_1 \perp d_1 \geq 0 \\
0 \leq d_2 + \psi_2 \perp d_2 \geq 0 \\
\vdots \\
0 \leq d_m + \psi_m \perp d_m \geq 0
\end{aligned}$$

$$\begin{aligned}
0 \leq d_1 + (c_2 + c_3 + \ldots + c_{m-1} + c_m) + \psi_1 \perp \lambda_1 \geq 0 \\
0 \leq d_2 + (c_2 + c_3 + \ldots + c_{m-1} + c_m) + \psi_2 \perp \lambda_2 \geq 0 \\
\vdots \\
0 \leq d_m + (c_2 + c_3 + \ldots + c_{m-1} + c_m) + \psi_m \perp \lambda_m \geq 0
\end{aligned}$$

$$0 \leq (c_2 + c_3 + \ldots + c_{m-1} + c_m) + \psi_1,$$

where

$$c_i = \max(0, \psi_1 - \psi_i), i = 2, \ldots, m, \tag{15}$$

and d are slack variables. Note that $\psi_i := [\psi_n]_i$. See [26] for further details of this derivation.

G. Polyhedral Exact Geometry Formulation of the Mixed Linear Complementarity System

The original Stewart-Trinkle forumation in (3) is altered to introduce a heuristic method based on the Polyhedral Exact Geometry formulation discussed in Section II-C. The main formulation becomes

$$\begin{vmatrix} 0 \\ \rho_n^{l+1} \\ \rho_a^{l+1} \end{vmatrix} = \begin{vmatrix} M & -G_n & 0 \\ G_n^T & 0 & E_1 \\ G_a^T & 0 & E_2 \end{vmatrix} \begin{vmatrix} v^{l+1} \\ p_n^{l+1} \\ c_a^{l+1} \end{vmatrix} + \begin{vmatrix} -Mv^l - p_{ext}^l \\ \Psi_n^l / h \\ \Psi_a / h \end{vmatrix}, \tag{16}$$

where M is the mass matrix, and G_n and G_a are the normal and auxiliary contact wrenches, respectively. Multiple adjacent contacts are grouped, and the components of G_n

from (4) are split into G_n and G_a in (16). G_n contains the contact wrenches of the contacts with the minimum value of ψ_n for each group of contacts. The remaining contact wrenches in each manifold are put into G_a. The auxiliary gap functions are defined as

$$\Psi_a = \begin{bmatrix} \Psi_{a_1} \\ \vdots \\ \Psi_{a_{n_s}} \end{bmatrix} \text{ where } \Psi_{a_j} = \begin{bmatrix} \Psi_1 - \Psi_2 \\ \vdots \\ \Psi_1 - \Psi_{n_s} \end{bmatrix}. \quad (17)$$

This employs a heuristic method, where only the closest constraint with a positive distance ψ_n is chosen as the active constraint. Further constraints are required to guarantee that only one constraint in each group of contacts is active at each instant. One normal contact wrench is put in $\mathbf{G}_n$ for each manifold, while all the other contact normals are put in the auxiliary wrench. The selection matrices apply the additional constraints to enforce that the correct constraint is active.

All elements of the component of the selection matrix E_{1_j} are equal to one, for each contact. The selection matrix E_2 is such that all E_{2_j} are equal to a lower triangular matrix where all nonzero values are equal to one.

The resulting size of the MCP system for the Polyhedral Exact Geometry method is $2 \cdot b + c$, where b is the number of active bodies, c is the total number of contacts.

III. Results

Two planar systems without friction are presented to compare the Stewart-Trinkle and Polyhedral Exact Geometry time-stepping methods. Both simulations involve a single particle interacting with bodies represented by vertices connected by edges. Contact in this case is unilateral only, and no other constraints are present. Standard Earth gravity acts downward in the $-Y$ direction in all simulations. All simulations were performed using the *minisim* component of the RPI Matlab Simulator [29].

A. Sawtooth Simulation

Two simulations are run to compare the performance of the Polyhedral Exact Geometry and the Stewart-Trinkle methods under varying conditions. A planar system consisting of a particle moving among multiple stationary bodies is used in this analysis. The particle has mass 5 kg, and an initial velocity of $\mathbf{0}$, unless otherwise stated. All surfaces are frictionless. System states are updated at each time-step with the results obtained by solving (3) or (16) with the PATH solver [27], [28].

1) Comparison of the Polyhedral Exact Geometry and Stewart-Trinkle methods: The simulated trajectories are shown in Figure 4. A single run using each method is depicted on the same plot. The particle starts at $[0.00, 0.75]$ meters, with an initial velocity of $[2.0, 1.8]$.

The trajectories are shown in more detail in Figure 5. The point near where the particle leaves the second ramp is examined. Using the Stewart-Trinkle method, the particle remains constrained past the boundary of the ramp. The value of ϵ is 0.25 meters; the effect of the constraint on the overall trajectory of the particle is significant. The particle leaves the

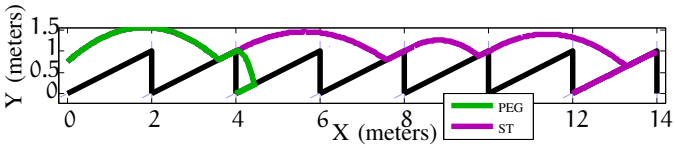

Fig. 4: *Trajectories of the Polyhedral Exact Geometry and Stewart-Trinkle methods*

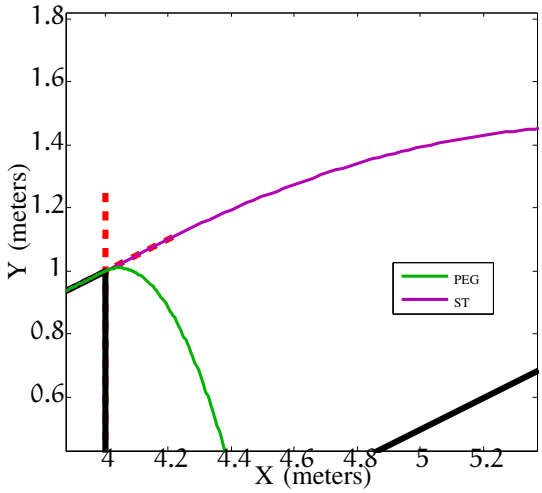

Fig. 5: *Detail of the trajectories in Figure 4*

sawtooth with a high velocity as it instantaneously enters a region in deep penetration of half space constraint resulting from the vertical edge.

The problem size at each time-step during the simulations is plotted in Figure 6. The problem size varies depending on the broad phase collision detection, and is the size of the main matrices in (3) and (16). Both methods start with no active constraints, giving the minimum problem size of 2, which corresponds with the size of the mass matrix.

Figure 7 shows the CPU time at each time-step for both methods. The required computation time generally corresponds with the problem size, with the Polyhedral Exact Geometry method being at a slight disadvantage at the low problem sizes in these small benchmark problems.

2) Comparison of different time-step sizes: The sawtooth simulation is run at multiple time-steps to compare the behavior of the Polyhedral Exact Geometry method and Stewart-Trinkle method under expected poor accuracy. Each simulation is run with step sizes of 1×10^{-4}, 1×10^{-3}, 1×10^{-2}, and 1×10^{-1}. The same parameters as in Section III-A.1 are used. Figure 8 illustrates the trajectories calculated for the two simulations. The trajectories for all time-steps

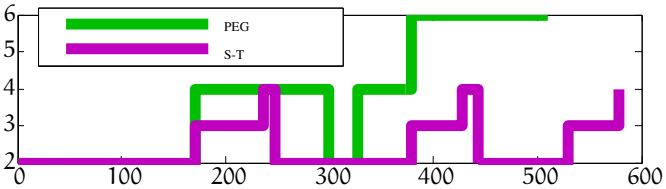

Fig. 6: *Problem size for the Polyhedral Exact Geometry and Stewart-Trinkle methods*

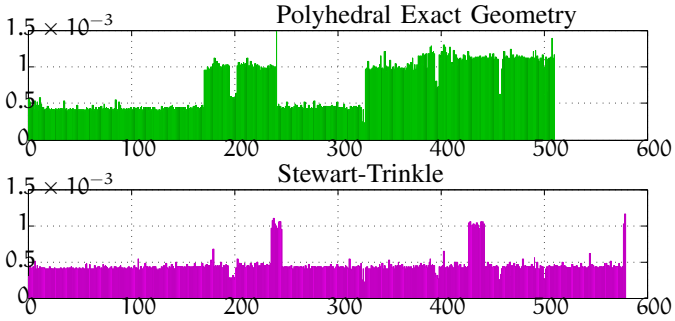

Fig. 7: *Solver time for the Polyhedral Exact Geometry and Stewart-Trinkle methods*

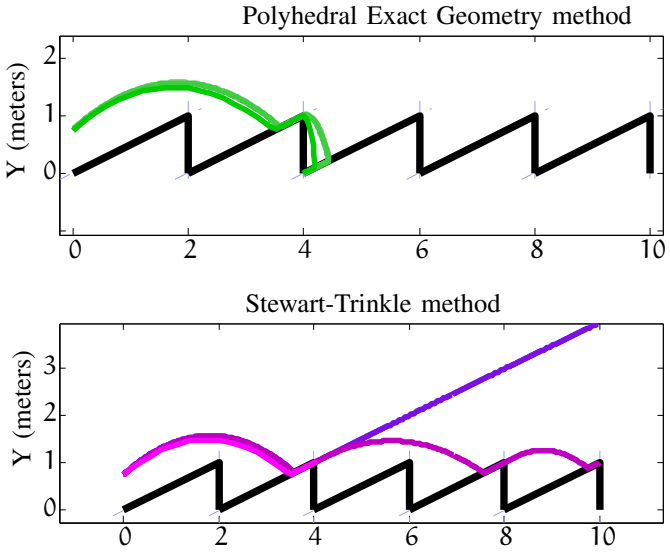

Fig. 8: *Trajectories of the Polyhedral Exact Geometry and Stewart-Trinkle methods under varying timesteps*

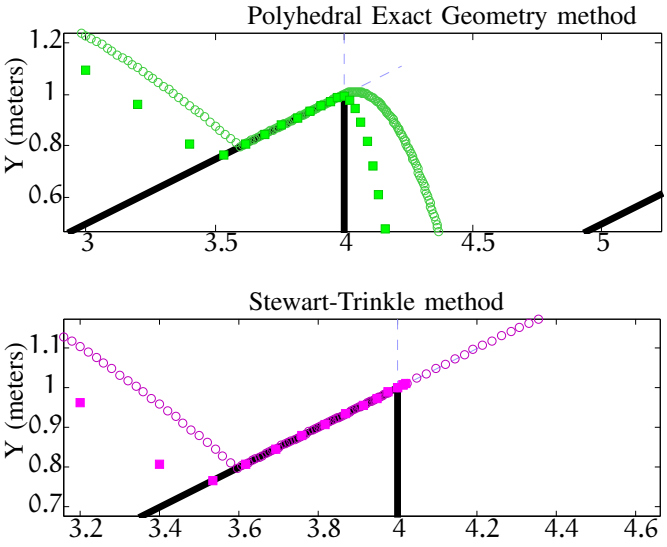

Fig. 9: *Detailed view of trajectories of the Polyhedral Exact Geometry and Stewart-Trinkle methods under varying timesteps*

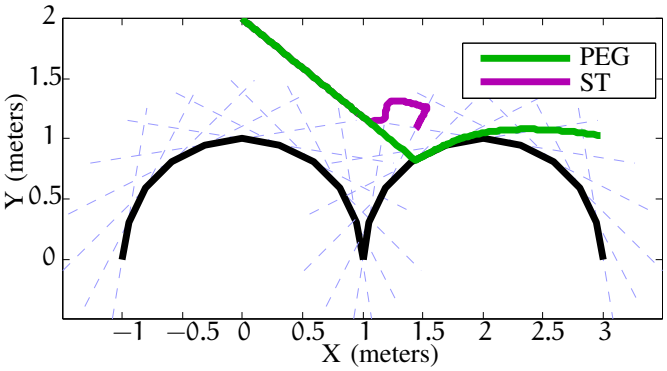

Fig. 10: *Trajectories of the Polyhedral Exact Geometry and Stewart-Trinkle methods*

in each method are shown. The trajectories at all time-steps are similar, except at the coarse value of 1×10^{-1}. In these cases, the trajectory differs from the trajectories in the other runs.

A detailed view of the trajectories in Figure 8 is presented in Figure 9. An area of interest near the peak of the first sawtooth encountered by the particle. The particle leaves the surface of the object as it travels in the $+$X direction in this region. For the cases with time-steps of 1×10^{-1} and $1 \times 10{-}2$, the individual positions are marked. The square markers correspond with the trajectory with a coarse time-step of 1×10^{-1}.

The lower subplot in Figure 9 shows a detail of the trajectories at different time-steps of the Stewart-Trinkle method. As in the Polyhedral Exact Geometry method, the coarse time-step produces a trajectory that varies significantly from the trajectories of the finer time-steps. The consideration of edges only within a distance ϵ causes variation in the trajectories after the particle leaves contact with the edge of the object. The coarse trajectory gets stuck at the intersection of the two extended edges, while the fine trajectory picks up additional kinetic energy and enters the ballistic phase with a high velocity.

B. Hills Simulation

A simulation is run with a series of hills as fixed obstacles. The hills are circular, and composed of 10 edges each. A constant external force of $(12, 0)$ N is applied, in addition to gravity. A time-step of 1×10^{-2} is used, and the particle starts at an initial position of 2 meters in the $+Y$ direction. The minimum value of ϵ increased to 0.5 m.

Figure 10 shows the trajectories for both the Polyhedral Exact Geometry and Stewart-Trinkle methods. The dashed lines represent the boundaries of the half-spaces projected outward from each edge in the bodies.

A detail of the same trajectory from Figure 10, resulting from the Stewart-Trinkle method is shown in Figure 11. The boundaries of the half-spaces that impede the motion of the particle are highlighted.

The particle initially interacts with a constraint from a horizontal constraint [in magenta], and subsequently comes into contact with the cyan half-space boundary on the left. Kinetic energy is picked up from this first interaction, as the particle enters the half-space from the side, resulting in

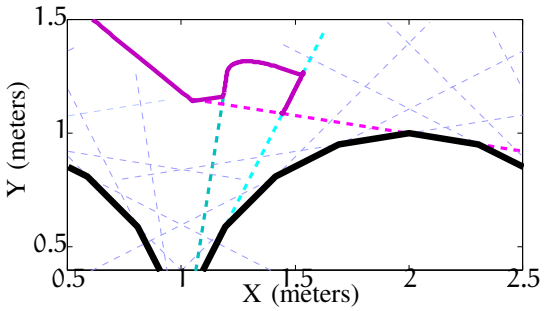

Fig. 11: *Detailed trajectory of Stewart-Trinkle method*

penetration as the constraint becomes active when the particle is within range ϵ. This phenomenon is discussed in detail in Section II-B. The high velocity, combined with the external force on the particle causes it to climb the boundary until the constraint becomes inactive as the distance from the right hill is greater than ϵ. After a brief phase of unconstrained motion, the constraint from the half-space edge depicted by the right cyan dashed line activates. The particle then travels a short distance down that constraint until meeting the constraint highlighted in magenta. The particle finally is trapped at the intersection of these two half-spaces.

IV. Conclusion

An analysis of improvements to simulation accuracy and performance utilizing the Polyhedral Exact Geometry method was performed in this work. The initial investigation was presented, with results obtained from small benchmark problems. Simulations consisting of a two dimensional particle with no friction were performed. The performance of the Polyhedral Exact Geometry method is similar to Stewart-Trinkle for these small benchmark problems, but it has been demonstrated that the Polyhedral Exact Geometry method is more robust, especially under consideration of tunable parameters in broad phase collision detection applied to the system before system dynamics are computed. The introduction of the Polyhedral Exact Geometry method in this work lays the foundation for further research into its performance on more complex 3D systems.

References

[1] H. Rahnejat, *Multi-body dynamics: vehicles, machines, and mechanisms*. Professional Engineering, 1998.

[2] R. Sinha, C. Paredis, V. Liang, and P. Khosla, "Modeling and simulation methods for design of engineering systems." *Journal of Computing and Information Science in Engineering(Transactions of the ASME)*, vol. 123, no. 1, pp. 84–91, 2001.

[3] P. Flores, R. Leine, and C. Glocker, "Application of the nonsmooth dynamics approach to model and analysis of the contact-impact events in cam-follower systems," *Nonlinear Dynamics*, vol. 69, no. 4, pp. 2117 – 2133, 2012.

[4] Z. Ma and N. Perkins, "An efficient multibody dynamics model for internal combustion engine systems," *Multibody system dynamics*, vol. 10, no. 4, pp. 363–391, 2003.

[5] N. Chakraborty, S. Berard, S. Akella, and J. Trinkle, "An implicit time-stepping method for quasi-rigid multibody systems with intermittent contact," vol. 5 PART A, Las Vegas, NV, United states, 2008, pp. 455 – 464.

[6] J. Sauer and E. Schömer, "A constraint-based approach to rigid body dynamics for virtual reality applications," in *Proceedings of the ACM symposium on Virtual reality software and technology*. ACM, 1998, pp. 153–162.

[7] "Bullet physics library," 2013. [Online]. Available: http://bulletphysics.org

[8] P. Lotstedt, "Coulomb friction in two-dimensional rigid body systems," *Zeitschrift fur Angewandte Mathematik und Mechanik*, vol. 61, no. 12, pp. 605 – 15, 1981.

[9] J. Trinkle, J.-S. Pang, J.-S. Sudarsky, and G. Lo, "On dynamic multi-rigid-body contact problems with coulomb friction," *Zeitschrift fur Angewandte Mathematik und Mechanik*, vol. 77, no. 4, pp. 267 – 79, 1997.

[10] L. Johansson, "Linear complementarity algorithm for rigid body impact with friction," *European Journal of Mechanics, A/Solids*, vol. 18, no. 4, pp. 703 – 717, 1999.

[11] W. Schiehlen, "Multibody system dynamics: Roots and perspectives," *Multibody system dynamics*, vol. 1, no. 2, pp. 149–188, 1997.

[12] B. Mirtich, "V-clip: fast and robust polyhedral collision detection," *ACM Trans. Graph.*, vol. 17, no. 3, pp. 177–208, Jul 1998.

[13] P. Jiménez, F. Thomas, and C. Torras, "3d collision detection: a survey," *Computers & Graphics*, vol. 25, no. 2, pp. 269–285, 2001.

[14] S. Redon, A. Kheddar, and S. Coquillart, "Fast continuous collision detection between rigid bodies," in *Computer graphics forum*, vol. 21, no. 3, 2003, pp. 279–287.

[15] D. Baraff, "Fast contact force computation for nonpenetrating rigid bodies," in *Proceedings of the 21st annual conference on Computer graphics and interactive techniques*. ACM, 1994, pp. 23–34.

[16] B. Mirtich and J. Canny, "Impulse-based simulation of rigid bodies," in *Proceedings of the 1995 symposium on Interactive 3D graphics*. ACM, 1995, pp. 181–ff.

[17] M. Anitescu and F. A. Potra, "Formulating dynamic multi-rigid-body contact problems with friction as solvable linear complementarity problems," *Nonlinear Dynamics*, vol. 14, pp. 231–247, 1997.

[18] D. Stewart and J. Trinkle, "An implicit time-stepping scheme for rigid body dynamics with inelastic collisions and coulomb friction," *International Journal for Numerical Methods in Engineering*, vol. 39, no. 15, pp. 2673 – 91, 8 1996.

[19] J. Trinkle, "Formulations of multibody dynamics as complementarity problems," in *Proceedings, ASME International Design Engineering Technical Conferences, September*, 2003.

[20] S. Berard, J. Trinkle, B. Nguyen, B. Roghani, J. Fink, and V. Kumar, "davinci code: A multi-model simulation and analysis tool for multi-body systems," in *Robotics and Automation, 2007 IEEE International Conference on*. IEEE, 2007, pp. 2588–2593.

[21] "Nvidia physx sdk," 2013. [Online]. Available: http://developer.nvidia.com/physx

[22] D. Stewart and J. Trinkle, "Implicit time-stepping scheme for rigid body dynamics with coulomb friction," in *Proceedings - IEEE International Conference on Robotics and Automation*, vol. 1, San Francisco, CA, USA, 2000, pp. 162 – 169.

[23] M. Anitescu and F. Potra, "A time-stepping method for stiff multi-body dynamics with contact and friction," *International Journal for Numerical Methods in Engineering*, vol. 55, no. 7, pp. 753 – 84, 11 2002.

[24] C. Bajaj and T. Dey, "Convex decomposition of polyhedra and robustness," *SIAM Journal on Computing*, vol. 21, no. 2, pp. 339–364, 1992.

[25] J. Lien and N. Amato, "Approximate convex decomposition of polyhedra," in *Proceedings of the 2007 ACM symposium on Solid and physical modeling*. ACM, 2007, pp. 121–131.

[26] B. Nguyen and J. Trinkle, "Modeling non-convex configuration space using linear complementarity problems," in *Proceedings - IEEE International Conference on Robotics and Automation*, Anchorage, AK, United states, 2010, pp. 2316 – 2321.

[27] M. Ferris and T. Munson, "Complementarity problems in gams and the path solver," *Journal of Economic Dynamics and Control*, vol. 24, no. 2, pp. 165 – 88, 2000.

[28] S. Dirkse, M. C. Ferris, and T. Munson, "The path solver," http://pages.cs.wisc.edu/ ferris/path.html, 2013. [Online]. Available: http://pages.cs.wisc.edu/ ferris/path.html

[29] J. Williams, Y. Lu, D. M. Flickinger, and J. Trinkle, "Rpi matlab simulator," http://code.google.com/p/rpi-matlab-simulator/, 2013. [Online]. Available: http://code.google.com/p/rpi-matlab-simulator/